Journal of Electroanalytical Chemistry 646 (2010) 133–141

Contents lists available at ScienceDirect

Journal of Electroanalytical Chemistry

journal homepage: www.elsevier.com/locate/jelechem

Enhancement of the second harmonic signal from $Hg_{1-x}Cd_xTe$ (MCT) in the presence of an anodic oxide film

A.W. Wark [a], K. McErlean [a], F.R. Cruickshank [a], L.E.A. Berlouis [a,*], P.F. Brevet [b]

[a] WestCHEM, Department of Pure and Applied Chemistry, University of Strathclyde, Glasgow G1 1XL, UK
[b] Laboratoire de Spectrometrie Ionique et Moleculaire, UMR CNRS 5579, Université Claude Bernard Lyon 1, 43 Boulevard du 11 Novembre 1918, 69622 Villeurbanne cedex, France

ARTICLE INFO

Article history:
Received 7 October 2009
Received in revised form 12 May 2010
Accepted 24 May 2010
Available online 1 June 2010

Keywords:
HgCdTe
Anodic oxide
Ellipsometry
SHG
Modeling

ABSTRACT

Second harmonic generation (SHG) is now widely regarded as a valuable tool for investigating electrode surfaces. Typically, most studies have been limited to substrates which lack bulk symmetry and monitoring events such as sub-monolayer formation and surface reconstruction. Here, the development of a model that can be used to quantitatively describe the enhanced SH signal observed in the presence of an anodic oxide film on a non-centrosymmetric substrate, $Hg_{1-x}Cd_xTe$ (MCT), is described. The aim is to further expand the utility of SHG for probing different electrode systems. The growth of the high quality oxide films was first followed by *in situ* ellipsometry. For thin films (<100 nm) grown at a constant current density of 150 μA cm^{-2}, an effectively uniform oxide layer is found with a refractive index n of ~2.15 ± 0.05 and exhibiting no absorption of the incident radiation at 632.8 nm (1.96 eV). In the presence of such an oxide film of 58 nm thickness, the second harmonic (SH) signal intensity measured in reflection is found to be significantly enhanced in both the P_{IN}–P_{OUT} and P_{IN}–S_{OUT} polarisation configurations. To quantify the changes observed, each layer in the model is assigned its own symmetry and optical constants at the fundamental, ω and harmonic Ω (= 2ω) frequencies and a defined thickness. Modeling of the SH rotational anisotropy experiments carried out at different angles of incidence indicated that most of this increase could be accounted for by multiple reflections of the fundamental wave ω = 1064 nm (1.17 eV) in the composite ambient/oxide/MCT layer, with little contribution from charge accumulation at the buried MCT/oxide interface for this oxide thickness.

1. Introduction

The alloy semiconductor $Hg_{1-x}Cd_xTe$ (MCT) is one of the most important materials used in the fabrication of infra-red devices [1]. By varying the composition x of this ternary compound semiconductor, the band-gap can be altered and thus allow the device to access different wavelengths in the infra-red region. One particular region of interest is the atmospheric transmission window between 8–12 μm wavelength and to access this, an alloy composition of x = 0.22 is employed. As with all devices based on the separation and flow of charge due to photon absorption, the electrical properties and efficiency of such devices have to be well characterised and controlled. However, the surface states present in such narrow gap semiconductors (for $x \sim 0.2$, E_g = 0.1 eV at 77 K) can dominate the desired properties of the material. Passivation layers [2] are employed to not only confer the correct degree of accumulation or flat band conditions to the MCT/passivant interface but also to provide chemical and physical protection during further processing and incorporation into the device. Typical surface passivation methodologies employed include the use of SiO_2 by photo-chemical vapour deposition [3], ZnS [4] as well as the native anodic oxides [5] and sulphides [6–8]. Anodic oxide layers are used in the passivation of photoconductors, leading to accumulation of the majority carrier at the surfaces of the n-type material. During the electrochemical formation of the anodic oxide layer, the MCT substrate material is consumed and sharp interfaces have thus been reported to form [2]. Oxide growth is usually carried out using the well established constant current anodisation method [5,9,10] in 0.1 M KOH in 90% ethylene glycol/10% H_2O.

Optical second harmonic generation (SHG) is a nonlinear process by which two photons at a fundamental frequency ω are converted into one photon at the harmonic frequency, $\Omega = 2\omega$. SHG by reflection has proven to be particularly useful as a surface or interface probe when the media are centrosymmetric and do not allow, in the dipole approximation, SHG from the bulk [11]. At any interface though, the inversion symmetry is broken, thus allowing SHG by reflection from such structures to be highly surface specific. For non-centrosymmetric materials, where bulk SHG is allowed, it would be expected that the bulk response would overwhelm this surface contribution. However, studies of non-centrosymmetric zinc blende-type materials by a number of workers [12–22] have

* Corresponding author. Tel.: +44 141 548 4244; fax: +44 141 548 4822.
E-mail address: l.berlouis@strath.ac.uk (L.E.A. Berlouis).

1572-6657/$ - see front matter © 2010 Elsevier B.V. All rights reserved.
doi:10.1016/j.jelechem.2010.05.013

also demonstrated a surface-sensitive SHG response in reflection. Both Stehlin et al. [12] and Buhaenko et al. [13] observed large variations in the reflected SH intensity during the vacuum deposition of tin and the adsorption of trimethylgallium on GaAs(0 0 1) surfaces respectively. Work by Armstrong et al. [23–26] showed that changes in both the rotational anisotropy pattern and a significant drop in the SH intensity could result on removal of a thin oxide overlayer. Rotational anisotropy studies by Yamada and Kimura [14–16] were able to demonstrate surface effects through surface reconstruction and, in their discussion of the relative bulk and surface contributions, included the possible mixing of the SHG response from two different faces through either miscuts or vicinal faces. Berlouis et al. [17–22] have shown that the use of SHG *in situ* was extremely useful in examining and characterising the growth of thin non-centrosymmetric anodic sulphide films on MCT.

The above studies have a direct relevance to the work presented here on the effect of the anodic oxide film on MCT. Whereas the MCT has a zinc-blende structure similar to that of GaAs, the anodic oxide consists of a mixture of $CdTeO_3$, $HgTeO_3$ and TeO_2 and is thus essentially centrosymmetic. Previous measurements on an oxide-covered MCT sample revealed that in the presence of the oxide film, the SH intensity was substantially increased over that of the bare MCT surface [27]. This observation suggests that SH generation within the MCT, at the MCT/oxide film and at film/air interfaces have all got to be carefully accounted for in order to quantify the various contributions to the observed SH signal from the oxide-covered MCT surface. The flexible multilayer model developed here expands on the work of Yamada and Kimura [16], where each layer is assigned its own symmetry and optical constants as well as a defined thickness. We note that for MCT, the reflected SHG signal is generated over a thin layer of material *ca.* 40–60 nm thick, known as the coupling depth, immediately at the interface [17].

2. Model geometry

The geometry described in Fig. 1 is general and can be extended to any number of layers where each layer is a semi-infinite parallel slab of a defined thickness, d_i. As described in the above figure the laboratory frame (0, *x*, *y*, *z*) is defined with the sample surface normal oriented along the *z* axis pointed upwards [28]. The *y* and *x* axes are oriented in the surface plane with the laboratory origin defined at the interface between medium 1 (representing air or electrolyte) and medium 2, with the top surface of the reflecting substrate at $z = 0$. The relationship between the laboratory and crystallographic axes will be defined later. Each slab is defined with its own complex refractive index, n_i^{ω} and n_i^{Ω} at the fundamental ω and harmonic $\Omega = 2\omega$ frequencies respectively.

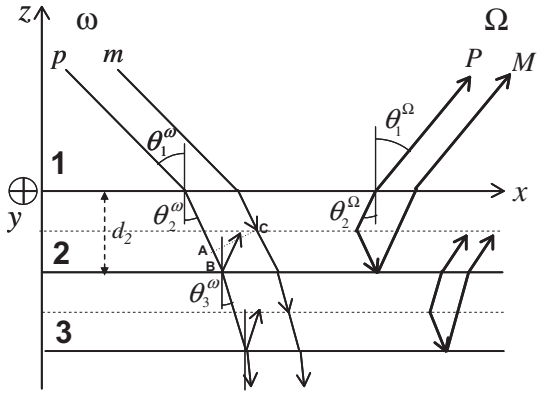

Fig. 1. Schematic of the different waves present within the multilayer model. For the layer of thickness d_2, the difference in geometrical path for reaching *C* directly or by reflection at the interface at *B* is $\delta^{\omega}_{path} = AB + BC$.

The fundamental wave is incident at the medium 1/medium 2 interface at an angle of θ_1^{ω}. Owing to the laws of refraction, the fundamental beam propagates within medium 2 at an angle θ_2^{ω} and θ_3^{ω} in medium 3 and so on. Similarly, the harmonic beam propagates at angles $\theta_1^{\Omega}, \theta_2^{\Omega}$ and θ_3^{Ω} all of which can be related using nonlinear Snell's law for SHG [29] where θ_1^{ω} is the incidence angle at the air/nonlinear material interface *i.e.*

$$n_1^{\omega}\sin\theta_1^{\omega} = n_2^{\omega}\sin\theta_2^{\omega} = n_2^{\Omega}\sin\theta_2^{\Omega} \tag{1}$$

Additionally, reflection and transmission at each interface is characterised using the Fresnel coefficients.

The complex expression for the incoming wave in medium 1 is

$$\boldsymbol{E}_{1-}(\boldsymbol{r},t) = \frac{1}{2}\{E_{1-}^{\omega}\hat{\boldsymbol{e}}_{1-}^{\omega}\exp(-i[\omega t - \boldsymbol{k}_{1-}^{\omega}\cdot\boldsymbol{r}]) + c.c.\} \tag{2}$$

with the sign +/− in the subscripts used to denote the direction of propagation: the negative sign for the wave propagating downwards, towards negative *z* values, and the positive sign for the wave propagating upwards, towards positive values of *z* in Fig. 1. $\hat{e}_{1-}^{\omega}$ thus represents a unit vector for the fundamental wave travelling in medium 1 towards the interface with medium 2. The different electric field vectors can be decomposed within medium *i* as

$$\boldsymbol{E}_{i-/+}^{\omega} = E_{is}^{\omega}\hat{\boldsymbol{s}} + E_{ip}^{\omega}\hat{\boldsymbol{p}}_{i-/+}^{\omega} \tag{3}$$

where the two unit vectors $\hat{\boldsymbol{s}}$ and $\hat{\boldsymbol{p}}_{i-/+}^{\omega}$ span the plane perpendicular to the direction of propagation and are defined according to

$$\hat{\boldsymbol{s}} = -\hat{\boldsymbol{y}} \tag{4}$$

$$\hat{\boldsymbol{p}}_{i-}^{\omega} = \cos\theta_i^{\omega}\hat{\boldsymbol{x}} + \sin\theta_i^{\omega}\hat{\boldsymbol{z}}$$

$$\hat{\boldsymbol{p}}_{i+}^{\omega} = -\cos\theta_i^{\omega}\hat{\boldsymbol{x}} + \sin\theta_i^{\omega}\hat{\boldsymbol{z}} \tag{5}$$

The polarisation of the incident fundamental electric field is defined through the relations:

$$\hat{\boldsymbol{s}}\cdot\hat{\boldsymbol{e}}_{1-}^{\omega} = \sin\gamma \tag{6}$$

$$\hat{\boldsymbol{p}}_{1-}^{\omega}\cdot\hat{\boldsymbol{e}}_{1-}^{\omega} = \cos\gamma e^{i\delta} \tag{7}$$

where γ is the angle of polarisation of the fundamental wave and δ is the dephasing angle between E_p^{ω} and E_s^{ω}. Corresponding values evaluated at the harmonic frequency is denoted with capital letters. These include Fresnel coefficients, polarisation angles and the $\widehat{\boldsymbol{P}}_i^{\Omega}$ and $\widehat{\boldsymbol{S}}$ unit vectors. For example the polarisation state of the outgoing SH wave is defined with angles of polarisation Γ and dephasing angle Δ as:

$$\widehat{\boldsymbol{S}}\cdot\hat{\boldsymbol{e}}_{1+}^{\Omega} = \sin\Gamma \tag{8}$$

$$\widehat{\boldsymbol{P}}_{1+}^{\Omega}\cdot\hat{\boldsymbol{e}}_{1+}^{\Omega} = \cos\Gamma e^{i\Delta} \tag{9}$$

For convenience, the propagating fundamental wave is described as the *m* wave in the downwards direction and the *p* wave in the upward direction. Similarly the downwards and upwards propagating harmonic waves are referred to as *M* or *P* respectively. The electric field vectors for these waves within medium 2 can be expressed as:

$$m\boldsymbol{e}_{2-}^{\omega} = (\hat{\boldsymbol{s}}t_{12}^{s}\hat{\boldsymbol{s}} + \hat{\boldsymbol{p}}_{2-}^{\omega}t_{12}^{p}\hat{\boldsymbol{p}}_{1-}^{w})\cdot\hat{\boldsymbol{e}}_{1-}^{\omega} \tag{10}$$

$$p\boldsymbol{e}_{2+}^{\omega} = (\hat{\boldsymbol{s}}t_{12}^{s}r_{23}^{s}\hat{\boldsymbol{s}} + \hat{\boldsymbol{p}}_{2+}^{\omega}t_{12}^{p}r_{23}^{p}\hat{\boldsymbol{p}}_{1-}^{w})\cdot\hat{\boldsymbol{e}}_{1-}^{\omega} \tag{11}$$

$$M\boldsymbol{e}_{2-}^{\Omega} = (\widehat{\boldsymbol{S}}T_{21}^{s}R_{23}^{s}\widehat{\boldsymbol{S}} + \widehat{\boldsymbol{P}}_{2-}^{\Omega}T_{21}^{p}R_{23}^{p}\widehat{\boldsymbol{P}}_{1+}^{\Omega})\cdot\hat{\boldsymbol{e}}_{1+}^{\Omega} \tag{12}$$

$$P\boldsymbol{e}_{2+}^{\Omega} = (\widehat{\boldsymbol{S}}T_{21}^{s}\widehat{\boldsymbol{S}} + \widehat{\boldsymbol{P}}_{2-}^{\Omega}T_{21}^{p}\widehat{\boldsymbol{P}}_{1+}^{\Omega})\cdot\hat{\boldsymbol{e}}_{1+}^{\Omega} \tag{13}$$

where the electric field vectors within medium 2 are now no longer unit vectors. For multiple layers additional Fresnel reflection (*r* and *R*) and transmission (*t* and *T*) coefficients are added to Eqs. (10)–(13) accordingly to describe the electric field vector for that layer. Thus through Eqs. (2)–(13), the directional and polarisation properties of the fundamental and harmonic waves can be fully expressed within